Article:

eprints@whiterose.ac.uk
https://eprints.whiterose.ac.uk/

Direct Writing of Elastic Fibers with Optical, Electrical, and Microfluidic Functionality

Markos Athanasiadis, Anna Pak, Dzmitry Afanasenkau, and Ivan R. Minev*

Direct Ink Writing is an additive fabrication technology that allows the integration of a diverse range of functional materials into soft and bioinspired devices such as robots and human-machine interfaces. Typically, a viscoelastic ink is extruded from a nozzle as a continuous filament of circular cross section. Here it is shown that a careful selection of printing parameters such as nozzle height and speed can produce filaments with a range of cross-sectional geometries. Thus, elliptic cylinder-, ribbon-, or groove-shaped filaments can be printed. By using the nozzle as a stylus for postprint filament modification, even filaments with an embedded microfluidic channel can be produced. This strategy is applied to directly write freeform and elastic optical fibers, electrical interconnects, and microfluidics. The integration of these components into simple sensor-actuator systems is demonstrated. Prototypes of an optical fiber with steerable tip and a thermal actuation system for soft tissues are presented.

Direct Ink Writing (DIW) is a simple, yet highly versatile additive fabrication technology. In a typical process, a viscoelastic material is extruded through a nozzle. The material, also referred to as ink, is laid down as a continuous filament by the translational motion of a robot creating structures in two or three dimensions. A broad array of materials has been employed in DIW. They often exhibit pronounced shear thinning behavior and can include colloidal suspensions, hydrogels, polymer precursors, or melts.[1] DIW is well suited for handling biomimetic materials such as elastomers and hydrogels, which is desirable for building bioinspired or biointegrated architectures.[2,3] Recently, inks with electrical functionality have made DIW an emerging technology for writing electrical circuits on mechanically conformable, dynamic, and stretchable substrates.[4–7] This can enable soft robots,[8] artificial sensing skins,[9] organ-on-chip platforms,[10] and bioelectronic implants.[11] Biological systems however are not just electrical machines. Devices engineered

to emulate or interface them, should possess multimodal sensing functionalities.[12–14] DIW is a promising technique for the creation of bioinspired systems comprising of sensors and actuators with electrical, optical, microfluidic, thermal, and mechanical functionalities.[15,16]

The resolution of the printing process is limited by the size of the extruded filament, which is typically circular in cross section, with diameter related to the nozzle's inner diameter. Strategies for controlling the cross-sectional geometry of extruded filaments such as custom nozzles with noncircular geometry are seldom explored, but could be a valuable approach to enhance the resolution and versatility of DIW.[17] Another interesting approach for enhancing print resolution beyond the nozzle size limitation was recently proposed by Yuk and Zhao who showed that a reduction of filament diameter could be achieved by stretching the filament during printing.[18]

Here we show that simple circular nozzles can be used to print filaments with ellipse, ribbon, groove, and even microchannel cross sections by harnessing deformation in the ink during printing. Producing these nonstandard filaments is achieved through rational control of printing parameters such as nozzle height and speed relative to the substrate. Using this approach we demonstrate a method to directly write elastic electrical interconnects, optical fibers, and microfluidic channels. We demonstrate their integration in soft systems for multimodal sensors and actuators.

In standard DIW operations, filaments have close to circular cross sections with diameter αd_{in}. Here d_{in} is the inner diameter of the nozzle and α is the die-swelling factor, which describes the postextrusion expansion of the ink.[19] Stable printing is achieved by setting the translational speed of the print head v to be close to the extrusion speed C, with which ink leaves the nozzle. At the same time, the height of the nozzle above the substrate h is kept similar to αd_{in} (**Figure 1**a). Following Yuk and Zhao, we introduce the dimensionless nozzle speed $V^* \equiv \frac{v}{C}$ and height $H^* \equiv \frac{h}{\alpha d_{in}}$ and point out that for conventional DIW with circular cross section filaments, both parameters are adjusted to be close to unity.[18] The extrusion speed C depends on the ink, nozzle, and applied pressure. For inks that age, C can change over time. Values for C and α are determined experimentally by printing simple test structures (Figure S1, Supporting Information).

As model inks, we use two different materials: SE1700 (Dow Corning), a printable silicone elastomer in the polydimethylsiloxane family and Carbopol (Lubrizol), a microgel based on cross

M. Athanasiadis, A. Pak, Dr. D. Afanasenkau, Dr. I. R. Minev
Biotechnology Center (BIOTEC)
Center for Molecular and Cellular Bioengineering (CMCB)
Technische Universität Dresden
Dresden 01307, Germany
E-mail: ivan.minev@tu-dresden.de

The ORCID identification number(s) for the author(s) of this article can be found under https://doi.org/10.1002/admt.201800659
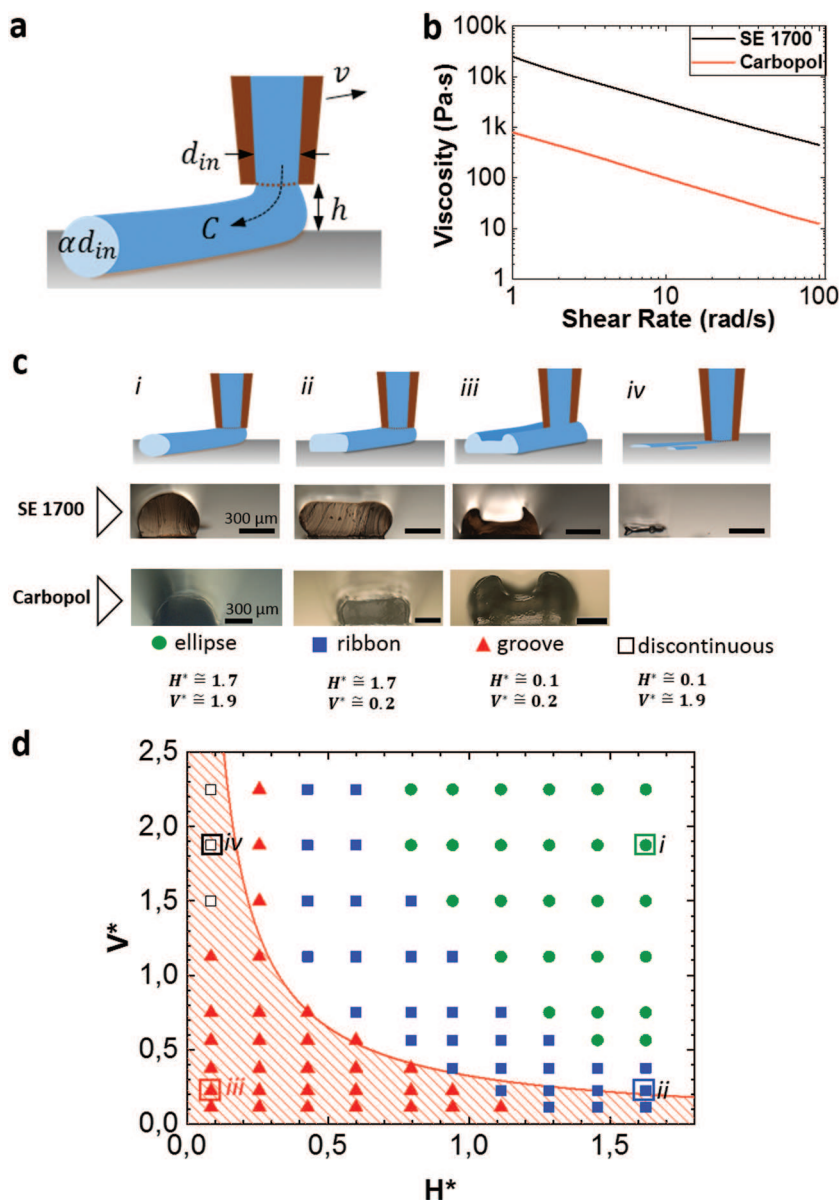
Figure 1. Nozzle speed and height control filament geometry. a) Schematic illustration of a typical DIW set-up. Key parameters that influence the extruded filament are the nozzle's inner diameter d_{in}, its height above the substrate h, and its translational speed v. b) As determined by oscillating plate rheometry, the two model inks SE1700 and Carbopol investigated here exhibit shear rate-dependent viscosity. c) Catalogue of filament cross sections produced by varying the speed and height of the print nozzle. Bottom row: optical micrographs of filaments printed with SE 1700 and with Carbopol. Filaments can be classified as (i) ellipse, (ii) ribbon, (iii) groove, and (iv) discontinuous. d) Phase diagram of transitions between the cross section geometries obtained with the SE1700 material. Data points in square boxes indicate the parameters used to produce the examples in (c). Filaments are identified as ribbon when the ratio between the width and height of cross sections is larger than 2. The shaded area indicates the parameter space for which Equation (1) predicts groove filaments.

linked polyacrylic acid.[20] Both inks exhibit shear rate-dependent viscosity (Figure 1b). This property allows for the ink to flow through the nozzle when pressure is applied and to "set" in the shape of a filament after the ink has exited the nozzle.

We start by noting that when H^* or V^* are close to or smaller than unity, noncircular cross section filaments are produced.

They can be described as elliptical cylinder, ribbon, groove, and discontinuous. The same combination of V^* and H^* produces a similar effect in both of our model inks (Figure 1c). To investigate how the interplay between, H^* and V^* influences which of the cross-sectional geometries is produced, we construct a phase diagram concentrating on the parameter space close to unity (Figure 1d). For these experiments, we use a nozzle with d_{in} and outer diameter d_{out} of 210 and 430 µm, respectively and SE1700. The phase diagram obtained with Carbopol appears nearly identical and is presented in Figure S2 in the Supporting Information.

When H^* or V^* are less than unity, the ink is squeezed and forced to deform between the nozzle and the substrate, which results in a filament flattened in the shape of a ribbon (Figure 1d, blue squares). Filaments are identified as ribbon when the ratio between the width and height of cross sections is larger than 2. By increasing V^* at a constant H^* we observe a gradual transition to ellipse and circular cross sections (e.g., Figure 1d, boxed symbols ii and i and Figure S3, Supporting Information). The transition between the ribbon and groove geometries is sharp and resembles a phase transition. Ribbon filaments become grooves when excess ink fully fills the space under the nozzle and starts to accumulate at the sides. Using an ink conservation argument, the condition for creating the groove filament can be expressed as follows

$$V^* \leq \frac{\pi}{4} \frac{d_{in}}{\alpha d_{out}} \frac{1}{H^*} \tag{1}$$

The phase boundary predicted by Equation (1) is presented as a solid red line in Figure 1d and Figure S2 in the Supporting Information and is in good agreement with experimental observations of ribbon versus groove filaments.

Next, we experiment with postextrusion modification of the filament cross section. To do this, we use the nozzle as a stylus by setting C to zero (no ink leaves the nozzle). Passing the stylus over a freshly printed (not yet polymerized) ribbon/ellipse filament of SE1700 silicone can create a groove in it (**Figure 2**). The width of the groove here is determined by d_{out}, the outer diameter of the printing nozzle. Shallow and deep grooves can be produced by programming the nozzle position above the substrate. Interestingly, we observed that engraving deep grooves causes collapse of their walls leaving behind a lumen. The lumen persists even after thermal polymerization of the ink.
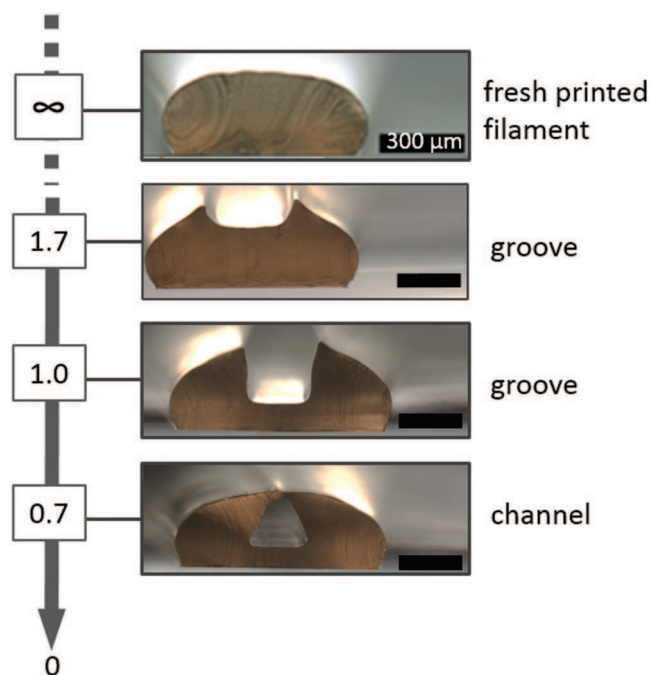
**ADVANCED
SCIENCE NEWS**

www.advancedsciencenews.com

**ADVANCED
MATERIALS
TECHNOLOGIES**

www.advmattechnol.de

Figure 2. Postextrusion modification of filament cross sections. Optical micrographs depicting the use of the printing nozzle as a stylus. Depending on the height of the stylus above the substrate (expressed in utits of H*), cross sectional geometries including grooves and channels can be produced with the SE1700 silicone.

Next, we combine ribbon and groove filaments to form functional core–shell fibers (**Figure 3**). As illustrated in Figure 3a, groove filaments can aid patterning a functional core material by restricting its spreading to the confines of the groove. Combined with a ribbon filament printed on top, the groove filaments serve as cladding protecting the core. In the case of conductive fibers the cladding functions as electrical insulation, in the case of optical fibers, it provides a step in refractive index. For optical fibers, we create a core by filling groove filaments with a high refractive index silicone (OE 6520, Dow Corning, RI = 1.54 compared to RI = 1.44 for SE 1700). The optical core cannot be printed as a continuous filament due to the low viscosity of the optical silicone. Instead, it is dosed (using a printing nozzle) inside the groove where it spreads. A ribbon filament is printed on top, acting as the optical seal. The entire fiber is then polymerized by heating. Optical fibers produced in this way display average attenuation of 0.72 ± 0.06 dB cm^{-1} (Figure S4, Supporting Information) for white light, which is similar to other polymer- or hydrogel-based waveguides fabricated by molding or soft lithography.[21–23] Printed optical fibers remain functional when tied in a knot, or when stretched to at least 30% tensile strain (Figure 3b). Strain of 30% results in 0.90 ± 0.03 fold change (decrease) of the transmitted optical power during the first stretch cycle. Within experimental error, strain-induced attenuation remains unchanged during the 1 000th stretch cycle. Similarly, electrical interconnects can be printed by filling groove filaments with a conductive material. Here we use compacted platinum microparticles as the conductive core while the groove and ribbon filaments act as electrical

passivation (Figure 3c). Elastic interconnects produced in this way display average conductivity of 22 ± 3.5 S cm^{-1} which is similar to the conductivity observed in other metal microparticle–based conductive composites.[24] Electrical interconnects remain conductive when stretched to at least 30% tensile strain (Figure 3d). Strain of 30% results in 6.80 ± 1.86 fold increase in resistance, which changes to 14.17 ± 2.02 after 1 000 strain cycles. Finally, we demonstrate that using the printing nozzle as a stylus, freeform microfluidic channels can be produced. Printed channels are observed to be free of obstructions (Figure 3e) and are able to support laminar flow (Figure S5, Supporting Information). The three types of fiber presented here exhibit nearly linear elasticity (up to at least 30% tensile strain) with elastic moduli in the range of 2.28–3.00 MPa, which is consistent with the behavior of the constituent silicone elastomers (Figure S6, Supporting Information).

Our DIW approach may enable direct writing of freeform arrays and integrated networks of functional fibers. Fibers themselves may perform multimodal sensing and actuating tasks, or they may link up nodes embedded in soft systems. Here we present two examples where fibers of different modalities are integrated. In the first demonstration, we fabricate an optical fiber with steerable tip that may find applications in endoscope systems with adaptive illumination.[25] We print a composite fiber consisting of a microfluidic channel on top of an optical core (**Figure 4**a). By blocking one end of the microfluidic channel and connecting the other to a syringe, we create a pneumatic actuator. Because of the off-axis position of the microfluidic channel, inflation with air results in bending of the entire structure and deflection of the tip of the optical fiber (Figure 4b). The applied pressure can control the amount of tip deflection (Figure 4c).

In our second demonstration, we fabricate a system for delivering and monitoring thermal modulation on soft curvilinear surfaces (**Figure 5**a). A microfluidic channel is printed in the shape of a flower. It circulates a liquid that facilitates thermal exchange. In the center we position a packaged digital temperature sensor interfaced with printed elastic interconnects. We apply our thermal actuator to the surface of a gelatin brain model. By flowing chilled ethanol at a rate of 1–2 mL min^{-1} through the thermal exchange loop, we achieved a temperature drop of 3.06 °C in the brain model as reported by the integrated temperature sensor (Figure 5b). Focal cooling of the cortical surface by only several degrees has been shown to be effective for seizure suppression in several species including humans.[26–28] Thermal neuromodulation is a promising strategy for treating intractable focal epileptic seizures that remains less investigated due to lack of suitable implantable technology.[29]

In summary, we demonstrate a strategy for rational control of the cross-sectional geometry of filaments printed with SE1700 silicone and Carbopol hydrogel. We integrate filaments in core–shell functional fibers and freeform microfluidics. As an alternative method to coextrusion with specialized coaxial nozzles, our approach relies on simple circular nozzles. Using groove and ribbon filaments we demonstrate production of fibers with optical, electrical, and microfluidic functionality. Freeform fibers may be integrated in webs of multimodal sensors and actuators. We envisage applications in soft robots as
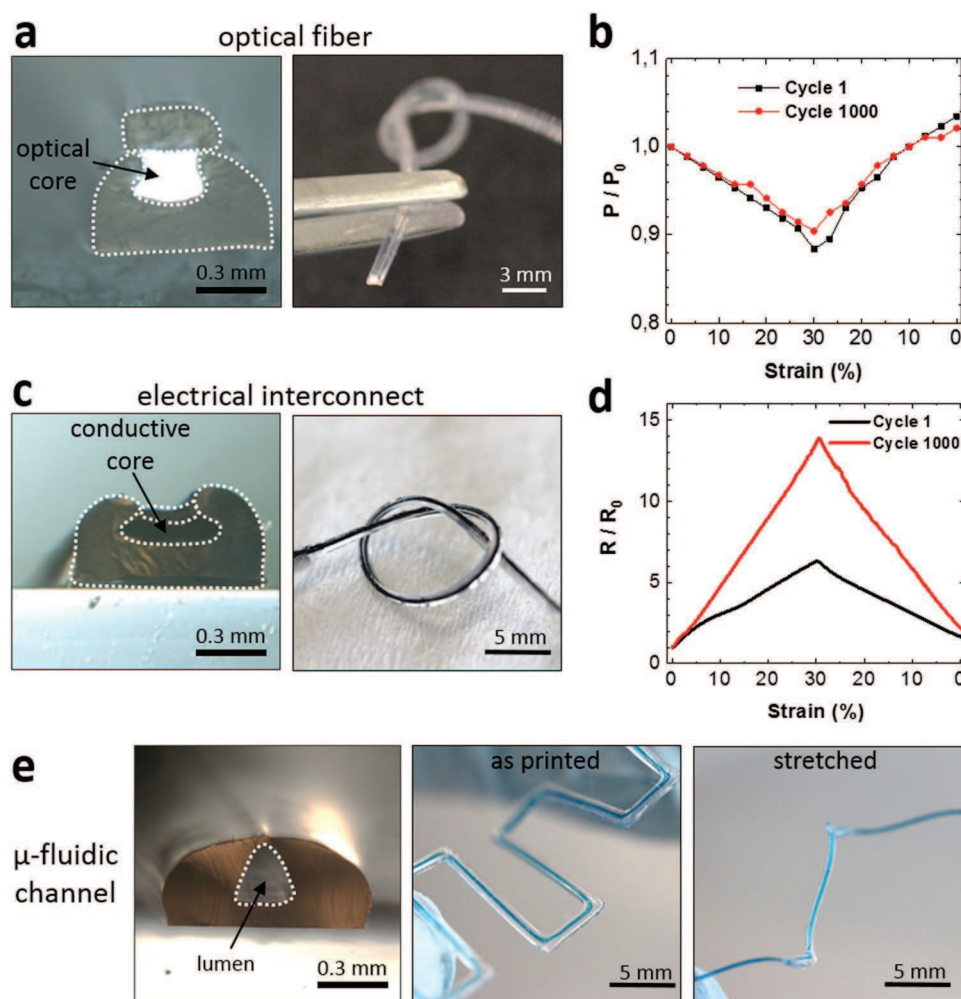
**ADVANCED
SCIENCE NEWS**

www.advancedsciencenews.com

**ADVANCED
MATERIALS
TECHNOLOGIES**

www.advmattechnol.de

Figure 3. Direct writing of functional elastic fibers. a) Micrographs of an optical fiber produced by combining filaments with groove and ribbon cross sections. The optical core is formed by a high refractive index silicone. The optical fiber is coupled to a white light source. b) Representative optical fiber subjected to tensile strain. The attenuation ratio $\frac{P}{P_0}$, is the ratio between transmitted power during stretch and at rest as measured at the fiber's free end. c) Micrographs of an electrical interconnect fiber. Here the groove is filled with platinum powder with average particle size of approximately 1 µm. d) Representative interconnect under tensile strain. Here $\frac{R}{R_0}$ is the ratio between the interconnect resistance at stretch and at rest. e) Micrographs of freeform microfluidics. As demonstrated by the infusion of a blue food dye, the channel lumen remains patent even at sharp turns of the fiber.

well as in implantable systems to deliver multimodal therapeutic programs to soft organs in the body.

Experimental Section

Ink Preparation: Silicone elastomers, SE 1700 and OE 6520 (Dow Corning), were prepared by mixing catalyst and base at a ratio of 1:10 and 1:1, respectively, followed by degassing. Carbopol (EDT 2020, Lubrizol Corporation) was prepared by vigorous mixing in water at a concentration of 2% w/w, followed by the addition of NaOH until pH 7.0 was achieved. For electrical interconnects, conductive ink was fabricated by mixing Platinum powder (particle diameter 0.2–1.8 µm, chemPUR, Germany) with tri(ethylene glycol) monoethyl ether (TGME, Merck KGaA) followed by sonication. The Platinum content in the suspension was around 15% by weight. The platinum suspension was deposited in groove filaments by ink-jet or by pipetting. The printed lines were then heated to 120 °C for 5 min to evaporate TGME leaving behind compacted dry Platinum powder inside groove filaments.

Printing: Printing was done using the 3D Discovery bioprinter from regenHU, Switzerland. Print layouts were developed in the BIOCAD software (regenHU). Studies of filament cross sections were conducted with the SE 1700 silicone and the Carbopol microgel. A plastic conical nozzle with nominal inner diameter of 200 µm at the tip (corrected to an actual value of 210 µm following precise optical measurements) was used. The pneumatic pressure was set at 5 and 1.2 bar for SE1700 and Carbopol, respectively. Printing of the platinum ink was done with the ink-jet printing head of the 3D Discovery instrument. The optical silicone OE 6520 was deposited by the nozzle extrusion method, using 100 µm inner diameter, metal nozzles (Poly Dispersing Systems). In all cases, the substrate used for printing was glass treated with 2% sodium dodecyl sulfate (Merck KGaA) to form a debonding layer.

Optical Fibers: To create a groove in a freshly printed filament of SE 1700 the nozzle ($d_{in} = 210$ µm, $d_{out} = 430$ µm) was used as a stylus. The groove filament was then heat cured at 120 °C for 45 min. One end of a cleaved silica optical fiber (ϕ 150 µm, Thorlabs) was placed inside the groove. Optical silicone (OE 6520) was then dispensed inside the groove to form the core of the optical fiber. This structure was heat cured at 120 °C for 45 min. A final ribbon-shaped filament of SE1700
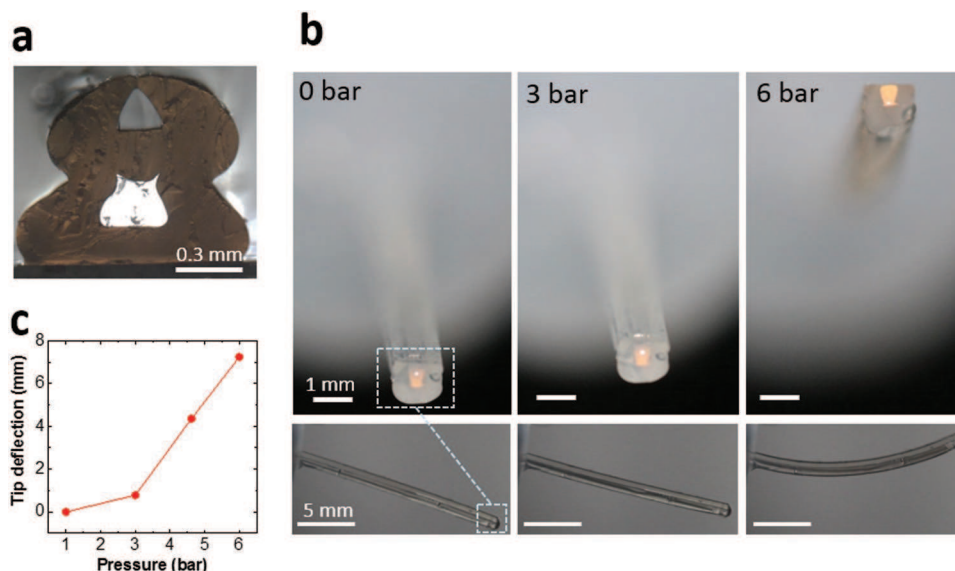
Figure 4. Integration of multimodal fibers by DIW. a) Cross section of a pneumatically actuated optical fiber illustrating the off-axis position of the microfluidic channel. b) Front (upper panels) and side (bottom panels) views of the actuator at rest and during the application of compressed air. c) °Quantification of tip deflection as a function of applied air pressure.

silicone formed a seal, and was heat cured at 120 °C for 45 min. Prior to each printing step, the structure was exposed to a brief oxygen plasma to improve interlayer adhesion. Finally, the free end of the silica optical fiber was coupled to a white light source (SCHOTT, KL 1500 electronic). Light transmission measurements were conducted by inserting the free end of the printed optical fiber into the opening of the integrating chamber of an optical power meter (PM100D, S142C, Thorlabs). For stretching experiments, the ends of printed fibers were attached to the prongs of a caliper.

Electrical Interconnects: Here a groove filament was filled with platinum ink by ink-jetting, and heated to 120 °C for 5 min to remove the dispersing solvent. A ribbon-shaped filament formed the electrical passivation. The two ends of the electrical interconnects were covered with, conductive epoxy (EPO-TEK H27D, Epoxy Technology) to which conventional electrical wires were attached. Printed electrical interconnects were stretched using a Dynamic Mechanical Analysis tester (SHIMADZU, EZ-SX) with a load cell of 20 N. During stretching, resistance measurements were performed using a potentiostat (AUTOLAB PGSTAT204, Metrohm).

Microfluidic Channel: Here, a nozzle (d_{in} = 210 µm, d_{out} = 430 µm) was used as a stylus passed through a freshly printed filament of SE 1700 silicone. In doing so, the walls of the groove-shaped filament collapse forming a triangular-shaped channel. The microfluidic channels were heat cured at 120 °C for 45 min.

Steerable Optical Fibers: A microfluidic channel was printed directly on top of an optical fiber. The end of the microfluidic channel was sealed with a small droplet of RTV silicone (734 Clear, Dow Corning). The other end was coupled to a needle mounted on a 6 mL syringe. The junction between the syringe and the microfluidic channel was secured with additional blobs of silicone. Air pressure was applied by depressing the syringe piston using a syringe pump (KD Scientific).

Thermal Modulation System: A microfluidic channel was printed in a flower shape. In the center of the flower a packaged digital temperature sensor (DS18B20, Maxim Integrated) was placed interfaced with printed electrical interconnects. The microfluidic channel was coupled with silicone tubes (Fredenberg Medical, Mono Lumen Tubing). The whole system was placed upon gelatin (Sigma-Aldrich, G1890-100G) cast in the shape of a hemisphere (red food dye is added to the gelatin). A
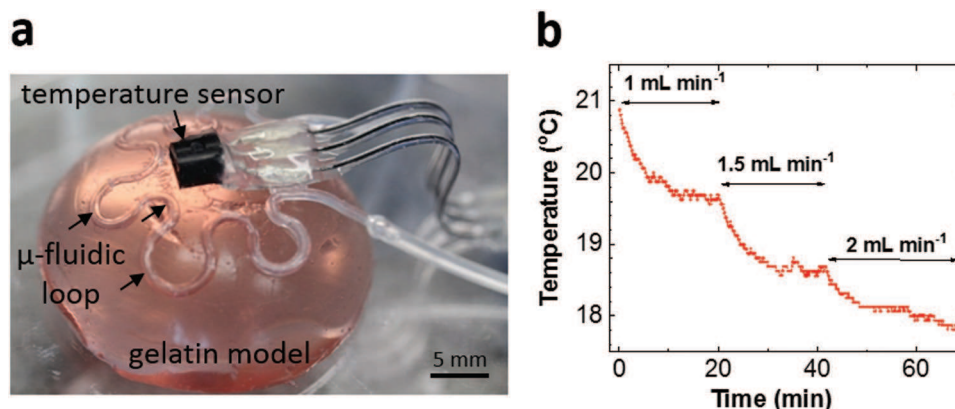

Figure 5. Demonstration of thermal actuation and sensing using printed fibers and a packaged sensor. a) A flower-shaped microchannel loop circulates thermal exchange liquid (ethanol). In the middle of the loop is a digital temperature sensor which is linked to printed electrical interconnects by conductive epoxy (EPO-TEK H27D). The sensor-actuator system conforms to the surface of a dome-shaped gelatin model of brain tissue. b) Thermal response of the model brain tissue to the circulation of chilled ethanol.

peristaltic pump (Bio-Rad, EP-1 Econo Pump) was used to pump chilled ethanol (−25 °C) through the microchannel network at different flow rates.

Imaging of Printed Structures: A ZEISS Discovery V2.0 microscope was used for the imaging of filament and fiber cross sections. Other optical images were captured with a macro lens.

Rheology Measurements: The rheology of SE1700 and Carbopol was investigated by oscillating plate rheometry (ARES, TA instruments, with parallel plates 8 mm of diameter). In order to quantify the shear-dependent viscosity behavior of the samples, the shear rate is stepped between 1 and 100 rad s^{-1}.

Statistics: Measurements were quoted as averages from at least three independent samples and errors represent standard deviation.

Supporting Information

Supporting Information is available from the Wiley Online Library or from the author.

Acknowledgements

Conflict of Interest

The authors declare no conflict of interest.

Keywords

[1] J. A. Lewis, *Adv. Funct. Mater.* **2006**, *16*, 2193.
[2] D. Espinosa-Hoyos, A. Jagielska, K. A. Homan, H. Du, T. Busbee, D. G. Anderson, N. X. Fang, J. A. Lewis, K. J. Van Vliet, *Sci. Rep.* **2018**, *8*, 478.
[3] A. Sydney Gladman, E. A. Matsumoto, R. G. Nuzzo, L. Mahadevan, J. A. Lewis, *Nat. Mater.* **2016**, *15*, 413.
[4] N. Matsuhisa, D. Inoue, P. Zalar, H. Jin, Y. Matsuba, A. Itoh, T. Yokota, D. Hashizume, T. Someya, *Nat. Mater.* **2017**, *16*, 834.
[5] M. S. Mannoor, Z. Jiang, T. James, Y. L. Kong, K. A. Malatesta, W. O. Soboyejo, N. Verma, D. H. Gracias, M. C. McAlpine, *Nano Lett.* **2013**, *13*, 2634.
[6] Y. Jo, J. Y. Kim, S.-Y. Kim, Y.-H. Seo, K.-S. Jang, S. Y. Lee, S. Jung, B.-H. Ryu, H.-S. Kim, J.-U. Park, Y. Choi, S. Jeong, *Nanoscale* **2017**, *9*, 5072.
[7] S. Y. Kim, K. Kim, Y. H. Hwang, J. Park, J. Jang, Y. Nam, Y. Kang, M. Kim, H. J. Park, Z. Lee, J. Choi, Y. Kim, S. Jeong, B. S. Bae, J. U. Park, *Nanoscale* **2016**, *8*, 17113.
[8] R. L. Truby, M. Wehner, A. K. Grosskopf, D. M. Vogt, S. G. M. Uzel, R. J. Wood, J. A. Lewis, *Adv. Mater.* **2018**, *30*, 1706383.
[9] J. T. Muth, D. M. Vogt, R. L. Truby, Y. Mengüç, D. B. Kolesky, R. J. Wood, J. A. Lewis, *Adv. Mater.* **2014**, *26*, 6307.
[10] J. U. Lind, T. A. Busbee, A. D. Valentine, F. S. Pasqualini, H. Yuan, M. Yadid, S.-J. Park, A. Kotikian, A. P. Nesmith, P. H. Campbell, J. J. Vlassak, J. A. Lewis, K. K. Parker, *Nat. Mater.* **2017**, *16*, 303.
[11] Z. Zhu, S.-Z. Guo, T. Hirdler, C. Eide, X. Fan, J. Tolar, M. C. McAlpine, *Adv. Mater.* **2018**, *30*, 1707495.
[12] B. W. An, J. H. Shin, S.-Y. Kim, J. Kim, S. Ji, J. Park, Y. Lee, J. Jang, Y.-G. Park, E. Cho, S. Jo, J.-U. Park, *Polymers* **2017**, *9*, 303.
[13] A. Canales, X. Jia, U. P. Froriep, R. A. Koppes, C. M. Tringides, J. Selvidge, C. Lu, C. Hou, L. Wei, Y. Fink, P. Anikeeva, *Nat. Biotechnol.* **2015**, *33*, 277.
[14] K. Kroll, M. Chabria, K. Wang, F. Häusermann, F. Schuler, L. Polonchuk, *Prog. Biophys. Mol. Biol.* **2017**, *130*, 212.
[15] A. D. Valentine, T. A. Busbee, J. W. Boley, J. R. Raney, A. Chortos, A. Kotikian, J. D. Berrigan, M. F. Durstock, J. A. Lewis, *Adv. Mater.* **2017**, *29*, 1703817.
[16] X. Liu, H. Yuk, S. Lin, G. A. Parada, T.-C. Tang, E. Tham, C. de la Fuente-Nunez, T. K. Lu, X. Zhao, *Adv. Mater.* **2018**, *30*, 1704821.
[17] R. B. Rao, K. L. Krafcik, A. M. Morales, J. A. Lewis, *Adv. Mater.* **2005**, *17*, 289.
[18] H. Yuk, X. Zhao, *Adv. Mater.* **2018**, *30*, 1704028.
[19] R. I. Tanner, *J. Polym. Sci., Part A-2: Polym. Phys.* **1970**, *8*, 2067.
[20] A. K. Grosskopf, R. L. Truby, H. Kim, A. Perazzo, J. A. Lewis, H. A. Stone, *ACS Appl. Mater. Interfaces* **2018**, *10*, 23353.
[21] J. Guo, X. Liu, N. Jiang, A. K. Yetisen, H. Yuk, C. Yang, A. Khademhosseini, X. Zhao, S.-H. Yun, *Adv. Mater.* **2016**, *28*, 10244.
[22] D. A. Chang-Yen, R. K. Eich, B. K. Gale, *J. Lightwave Technol.* **2005**, *23*, 2088.
[23] A. Ersen, M. Sahin, *J. Biomed. Opt.* **2017**, *22*, 055005.
[24] S. Lee, J. Koo, S.-K. Kang, G. Park, Y. J. Lee, Y.-Y. Chen, S. A. Lim, K.-M. Lee, J. A. Rogers, *Mater. Today* **2018**, *21*, 207.
[25] H. Bansal, S. Swain, G. K. Sharma, M. Mathanya, S. Trivedi, U. S. Dwivedi, P. B. Singh, *J. Endourology* **2011**, *25*, 317.
[26] K. M. Karkar, P. A. Garcia, L. M. Bateman, M. D. Smyth, N. M. Barbaro, M. Berger, *Epilepsia* **2002**, *43*, 932.
[27] H. Kida, M. Fujii, T. Inoue, Y. He, Y. Maruta, S. Nomura, K. Taniguchi, T. Ichikawa, T. Saito, T. Yamakawa, M. Suzuki, *Clin. Neurophysiol.* **2012**, *123*, 1708.
[28] S. M. Rothman, *Neurotherapeutics* **2009**, *6*, 251.
[29] S. M. Rothman, M. D. Smyth, X.-F. Yang, G. P. Peterson, *Epilepsy Behav.* **2005**, *7*, 214.